

The Discontinuous Asymptotic Telegrapher's Equation (P_1) Approximation

Avner P. Cohen,^{1,*} Roy Perry,² and Shay I. Heizler^{1,†}

¹*Department of Physics, Nuclear Research Center-Negev, P.O. Box 9001, Beer-Sheva 84190, ISRAEL*

²*Department of Physics, Ben-Gurion University, Beer-Sheva 84105, ISRAEL*

Modeling the propagation of radiative heat-waves in optically thick material using a diffusive approximation is a well-known problem. In optically thin material, classic methods, such as classic diffusion or classic P_1 , yield the wrong heat wave propagation behavior, and higher order approximation might be required, making the solution harder to obtain. The asymptotic P_1 approximation [Heizler, *NSE* 166, 17 (2010)] yields the correct particle velocity but fails to model the correct behavior in highly anisotropic media, such as problems that involve sharp boundary between media or strong sources. However, the solution for the two-region Milne problem of two adjacent half-spaces divided by a sharp boundary, yields a discontinuity in the asymptotic solutions, that makes it possible to solve steady-state problems, especially in neutronics. In this work we expand the time-dependent asymptotic P_1 approximation to a highly anisotropic media, using the discontinuity jump conditions of the energy density, yielding a modified discontinuous P_1 equations in general geometry. We introduce numerical solutions for two fundamental benchmarks in plane symmetry. The results thus obtained are more accurate than those attained by other methods, such as Flux-Limiters or Variable Eddington Factor.

I. INTRODUCTION

Radiation heat waves (Marshak waves) play important roles in many high energy density physical phenomena, for example in inertial confinement fusion (ICF) and in astrophysical and laboratory plasmas [1–4]. This problem has long been a subject of theoretical astrophysics research [5, 6], and of experimental studies testing radiative-hydrodynamics macroscopic modeling [7, 8]. Specifically, the propagating radiative Marshak waves in optically thick media are well described by a simple local thermodynamic equilibrium (LTE) diffusion model, yielding self-similar solutions of both supersonic and subsonic regimes [9–12]. However, in optically thin media, the diffusion limit fails to describe the exact physical behavior of the problem. In the general case, the propagation of the radiation is modeled via the Boltzmann (transport) equation for photons, coupled to the matter via the energy balance equation. In the gray (mono-energetic) radiation case the equation is:

$$\begin{aligned} \frac{1}{c} \frac{\partial I(\hat{\Omega}, \vec{r}, t)}{\partial t} + \hat{\Omega} \cdot \vec{\nabla} I(\hat{\Omega}, \vec{r}, t) + (\sigma_a(T_m(\vec{r}, t)) + \sigma_s(T_m(\vec{r}, t))) I(\hat{\Omega}, \vec{r}, t) = \\ \sigma_a(T_m(\vec{r}, t)) B(T_m(\vec{r}, t)) + \\ \frac{\sigma_s(T_m(\vec{r}, t))}{4\pi} \int_{4\pi} I(\hat{\Omega}, \vec{r}, t) d\hat{\Omega} + S(\hat{\Omega}, \vec{r}, t) \end{aligned} \quad (1)$$

where $I(\hat{\Omega}, \vec{r}, t)$ is the specific intensity of radiation at position \vec{r} propagating in the $\hat{\Omega}$ direction at time t . $B(T_m(\vec{r}, t))$ is the thermal material energy, where $T_m(\vec{r}, t)$ is the material temperature, c is the speed of light and $S(\hat{\Omega}, \vec{r}, t)$ is an external radiation source. $\sigma_a(T_m(\vec{r}, t))$ and $\sigma_s(T_m(\vec{r}, t))$ are the absorption (opacity) and scattering cross-sections respectively. In this paper we focus on the gray case, when the expansion to multi-energy approximation is straightforward [13]. Along with the equation for the radiation energy, the complementary equation for the material is:

$$\frac{C_v(T_m(\vec{r}, t))}{c} \frac{\partial T_m(\vec{r}, t)}{\partial t} = \sigma_a(T_m(\vec{r}, t)) \left(\frac{1}{c} \int_{4\pi} I(\hat{\Omega}, \vec{r}, t) d\hat{\Omega} - aT_m^4(\vec{r}, t) \right) \quad (2)$$

where $C_v(T_m(\vec{r}, t))$ is the heat capacity of the material.

Solving the transport equation is complicated, especially in multi-dimensions, where an exact solution is hard to obtain. The P_N approximation, which decomposes $I(\hat{\Omega}, \vec{r}, t)$ to its first N angular moments (defines N coupled equations, assuming the P_N closure), and the S_N method (the transport equation in N discrete ordinates), are

* avnerco@gmail.com

† highzlers@walla.co.il

deterministic methods, and they are both exact when $N \rightarrow \infty$ [13]. Alternatively, a statistical implicit Monte Carlo (IMC) approach can also be used [14], which is exact when the number of particles (histories) goes to infinity. Although these three methods approach the exact solution, their application requires extensive numerical calculations that might be difficult to carry out, especially in multi-dimensions. Hence, there is an extensive body of literature dealing with the search for approximate models which will be relatively easy to simulate, and yet produce solutions that are close to the exact problem (for example, see [15, 16]).

The classical (Eddington) diffusion theory, as a specific case of the P_1 is relatively easy to solve and is commonly used [1, 4, 13]. The diffusion equation is parabolic, and thus yields infinite particle velocities. The full P_1 equations, that give rise to the Telegrapher's equation, has a hyperbolic form, but with an incorrect finite velocity, $c/\sqrt{3}$ [17]. Possible solutions, such as flux-limiters (FL) solution (in the form of a non-linear diffusion notation), or Variable Eddington Factor (VEF) approximations (in the form of full P_1 equations), yielding a gradient-dependent nonlinear diffusion coefficients (or a gradient-dependent Eddington factor), are harder to solve, especially in multi-dimensions [15, 16, 18–24].

In previous work, Heizler [17] offered a modified P_1 approximation, based on the asymptotic derivation (both in space and time), the asymptotic P_1 approximation (or the asymptotic Telegrapher's equation approximation) [17]. In steady state, it tends to the well-known asymptotic diffusion approximation [13, 25, 26]. This approximation shares similar asymptotic behavior with the SP_2 approximation in highly isotropic problems [27]. It was tested in radiation problems under the *LTE* assumption, yielding relatively good results, especially near the tails, but also producing significant deviations in the regions where the material and radiation temperatures differ significantly [28].

However, when the radiation intensity is highly anisotropic, for example near a sharp boundary between two different media or near strong sources, the asymptotic P_1 results, are almost as poor as the classic P_1 or asymptotic diffusion approximations. Similar problem occurred in neutronics, with a sharp boundary of two different media, such as reactor-reflector problems [29]. This problem can be corrected by using the exact solution to obtain the exact scalar flux and the neutron current, on the boundary between the two media, yielding a discontinuous asymptotic diffusion theory [30–34]. This correction is the two-region extension to the classic radiative transfer Milne problem [1, 6], that has its origins in the attempt to calculate the distribution of light emitted from the photosphere of a star. The problem can be solved where the star is modeled as a semi-infinite half-space (with a vacuum boundary condition). By this correction, the problem of steady-state critical values in reactor-reflector problems is accurately modeled [29]. We note that Zimmerman [35] offered an approximate version of this solution, based on the two-region Marshak-like boundary condition [13], in order to adjust the different zones. In his approach the scalar flux has a discontinuity on the boundary, but the neutron current is continuous (and thus conserves particles).

In this work we offer a time-dependent version of this approach, i.e. expanding the asymptotic P_1 approximation to a non-homogeneous space problem. By assuming that the energy density (the zero's moment of the specific intensity $I(\hat{\Omega}, \vec{r}, t)$) has a discontinuity, we derive the *discontinuous asymptotic Telegrapher's equation (P_1) approximation*. Our new method will be compared to other known diffusion and flux-limiter approximations, as well as the P_1 approximation and the VEF approximations in two basic and important problems: The Su-Olson (constant opacity) benchmark [36, 37], and the nonlinear-opacity Olson's benchmark [15]. It is important to note that the extension of the discontinuous asymptotic P_1 approximation is also straightforward for neutronics.

The present paper is structured in the following manner: first, in Sec. II we will introduce common approximations for the Boltzmann equation. In Sec. III we present the derivation of the discontinuous asymptotic Telegraphers equation (P_1) approximation. Next, in Sec. IV the various approximations will be tested in the well-known radiation benchmarks. In Sec. V we examine another version of a discontinuous P_1 approximation, forcing a discontinuity in both energy density and radiation flux. A short discussion is presented in Sec. VI.

II. APPROXIMATE MODELS FOR THE RADIATIVE TRANSFER EQUATION

The first two angular moments of the specific intensity $I(\hat{\Omega}, \vec{r}, t)$ can be expressed as:

$$E(\vec{r}, t) = \frac{1}{c} \int_{4\pi} I(\hat{\Omega}, \vec{r}, t) d\hat{\Omega} \quad (3)$$

$$\vec{F}(\vec{r}, t) = \int_{4\pi} I(\hat{\Omega}, \vec{r}, t) \hat{\Omega} d\hat{\Omega} \quad (4)$$

where $E(\vec{r}, t)$ is the energy density, and $\vec{F}(\vec{r}, t)$ is the radiation flux.

Integration Eq. 1 over all solid angle $\int d\hat{\Omega}$ yields *the conservation law*:

$$\frac{1}{c} \frac{\partial E(\vec{r}, t)}{\partial t} + \frac{1}{c} \nabla \cdot \vec{F}(\vec{r}, t) = \sigma_a(T_m(\vec{r}, t)) \left(\int_{4\pi} \frac{B(\vec{r}, t)}{c} d\hat{\Omega} - E(\vec{r}, t) \right) + \frac{S(\vec{r}, t)}{c} \quad (5)$$

Integration Eq. 1 with $\int \hat{\Omega} d\hat{\Omega}$ yields:

$$\frac{1}{c} \frac{\partial \vec{F}(\vec{r}, t)}{\partial t} + c \vec{\nabla} \cdot \int_{4\pi} I(\hat{\Omega}, \vec{r}, t) \hat{\Omega} d\hat{\Omega} + \sigma_t(T_m(\vec{r}, t)) F(\vec{r}, t) = 0 \quad (6)$$

when $\sigma_t(T_m(\vec{r}, t)) = \sigma_a(T_m(\vec{r}, t)) + \sigma_s(T_m(\vec{r}, t))$ is the total cross-section. Eqs. 5 and 6 are exact equations. In these equations there are 3 unknown moments of $I(\hat{\Omega}, \vec{r}, t)$, but only two equations. Hence, we have to assume a closure for this moments representation, i.e. to introduce an approximation for the third moment: $\int_{4\pi} I(\hat{\Omega}, \vec{r}, t) \hat{\Omega} d\hat{\Omega}$. In the following we introduce a set of approximations that retain the conservation law (Eq. 5) (allowing energy conservation), while an approximation is introduced for Eq. 6 (and for the third moment).

A. The Classic Diffusion and P_1 (Telegrapher's Equation) Approximations

The classic diffusion (or the classic Eddington) approximation (which is a simplification of the P_1 approximation) is the most well-known approximation for the Boltzmann (transport) equation [13] and is extensively used, especially in radiative transfer equation (RTE).

In the derivation of the P_1 approximation, one assumes that $I(\hat{\Omega}, \vec{r}, t)$ is a sum of its first two moments. Therefore the third moment can be approximated as $\int_{4\pi} I(\hat{\Omega}, \vec{r}, t) \hat{\Omega} d\hat{\Omega} \approx E(\vec{r}, t)/3$. In this case, Eq. 6 takes this form:

$$\frac{1}{c} \frac{\partial \vec{F}(\vec{r}, t)}{\partial t} + \frac{c}{3} \vec{\nabla} E(\vec{r}, t) + \sigma_t(T_m(\vec{r}, t)) \vec{F}(\vec{r}, t) = 0 \quad (7)$$

Eqs. 5 and 7, defining the P_1 approximation, are a set of two closed equations for $E(\vec{r}, t)$ and $\vec{F}(\vec{r}, t)$, coupled with the material energy equation, Eq. 2.

If the derivative of the energy flux $\vec{F}(\vec{r}, t)$ with respect to time inside Eq. 7 is negligible, a form of a Fick's law is obtained:

$$\vec{F}(\vec{r}, t) = -cD(\vec{r}, t) \vec{\nabla} E(\vec{r}, t), \quad (8)$$

where $D(\vec{r}, t) = 1/[3\sigma_t(T_m(\vec{r}, t))]$. Substituting Eq. 8 in Eq. 5 gives a diffusion equation:

$$\frac{1}{c} \frac{\partial E(\vec{r}, t)}{\partial t} - \vec{\nabla} \cdot \left(D(\vec{r}, t) \vec{\nabla} E(\vec{r}, t) \right) = \sigma_a(T_m(\vec{r}, t)) \left(\frac{B(\vec{r}, t)}{c} - E(\vec{r}, t) \right) + \frac{S(\vec{r}, t)}{c} \quad (9)$$

We note that the classic diffusion approximation yields a wrong time-description due to its parabolic nature; the diffusion approximation yields an infinite particle velocity. The full P_1 approximation (Eqs. 7 and 5) can be reformulated in a hyperbolic form:

$$\begin{aligned} & \frac{1}{c\sigma_t(T_m(\vec{r}, t))} \frac{\partial^2 E(\vec{r}, t)}{\partial t^2} - \frac{c}{3} \cdot \nabla \cdot \frac{1}{\sigma_t(T_m(\vec{r}, t))} \nabla E(\vec{r}, t) + \frac{\partial E(\vec{r}, t)}{\partial t} + \\ & \frac{1}{\sigma_t(T_m(\vec{r}, t))} \frac{\partial (\sigma_a(T_m(\vec{r}, t)) E(\vec{r}, t))}{\partial t} + \sigma_a(T_m(\vec{r}, t)) c E(\vec{r}, t) = \\ & 4\pi \sigma_a(T_m(\vec{r}, t)) B(\vec{r}, t) + S(\vec{r}) + \frac{4\pi}{c\sigma_t(T_m(\vec{r}, t))} \frac{\partial (\sigma_a(T_m(\vec{r}, t)) B(\vec{r}, t))}{\partial t} + \frac{1}{\sigma_t(T_m(\vec{r}, t))} \frac{\partial S(\vec{r}, t)}{\partial t} \end{aligned} \quad (10)$$

The equation is developed under the assumption that both time derivative of $\vec{F}(\vec{r}, t)$ and the opacity spatial change are small enough, so the $\vec{\nabla} \cdot \left(\frac{1}{\sigma_t(T_m(\vec{r}, t))} \right) \cdot \frac{\partial \vec{F}(\vec{r}, t)}{\partial t}$ term, can be neglected [17, 28]. This equation is called the Telegrapher's equation, and it combines both the second and the first derivative of the energy density with respect to time. The particle velocity in the classic P_1 approximation is too small, $c/\sqrt{3}$ [17, 28], unlike the classic diffusion particle velocity which is too fast.

B. Flux-limiter diffusion and Variable Eddington factor approximations

The parabolic nature of the diffusion approximation can be corrected by using a nonlinear diffusion coefficient; flux-limited diffusion coefficient [15, 16, 21, 23]. This method limits the diffusion coefficients so that particles diffusion velocity will not diverge. For example, the diffusion coefficient in Larsen's *ad hoc* flux limiter (FL) is [15]:

$$D(\vec{r}, t) = \left[(3\sigma_t(T_m(\vec{r}, t)))^n + \left(\frac{1}{E(\vec{r}, t)} \frac{\partial E(\vec{r}, t)}{\partial x} \right)^n \right]^{-1/n} \quad (11)$$

If the gradient of $E(\vec{r}, t)$ is small, the diffusion coefficient tends to the classic value of diffusion theory, $D(\vec{r}, t) = 1/[3\sigma_t(T_m(\vec{r}, t))]$. If the gradient of $E(\vec{r}, t)$ is large, Eq. 11 limits the diffusion coefficient, forcing $F(\vec{r}, t) \leq cE(\vec{r}, t)$. Using $n = 1$ this Flux-limiter tends to Wilson-sum FL, and taking $n \rightarrow \infty$, it tends to Wilson-Max FL [21].

There are various versions of different Flux-Limiters [15, 16, 21, 23], some of them are more physically-based than others. For example, we introduce here the well-known Levermore-Pomraning (LP) [20, 24]. By defining of $\omega_{\text{eff}}(\vec{r}, t)$, the mean number of particles emitted per collision as:

$$\omega_{\text{eff}}(\vec{r}, t) = \frac{\sigma_s(T_m(\vec{r}, t))E(\vec{r}, t) + \sigma_a(T_m(\vec{r}, t))B(\vec{r}, t) + S(\vec{r}, t)/c}{\sigma_t E(\vec{r}, t)}, \quad (12)$$

and the normalized radiation energy density gradient $R(\vec{r}, t)$ as:

$$R(\vec{r}, t) = \frac{|\vec{\nabla} E(\vec{r}, t)|}{\omega_{\text{eff}}(\vec{r}, t)\sigma_t(T_m(\vec{r}, t))E(\vec{r}, t)} \quad (13)$$

the diffusion coefficient ($D(\vec{r}, t)$) in Eq. 8 and Eq. 9 takes the form:

$$D(\vec{r}, t) = \frac{\lambda(R(\vec{r}, t))}{\omega_{\text{eff}}(\vec{r}, t)} \quad (14)$$

where $\lambda(R(\vec{r}, t))$ is:

$$\lambda(R(\vec{r}, t)) = \left[\coth(R(\vec{r}, t)) - \frac{1}{R(\vec{r}, t)} \right] \frac{1}{R(\vec{r}, t)} \quad (15)$$

Another class of approximations is the variable Eddington factor (VEF) approximations. In these approximations, that have a P_1 notation, the second-moment term in Eq. 6 is approximated with an Eddington Factor (EF), $\chi(\vec{r}, t)$:

$$\frac{1}{c} \frac{\partial F(\vec{r}, t)}{\partial t} + c\vec{\nabla}(\chi(\vec{r}, t)E(\vec{r}, t)) + \sigma_t(T_m(\vec{r}, t))F(\vec{r}, t) = 0, \quad (16)$$

where $\chi(\vec{r}, t)$ is called the Eddington factor (EF). The EF depends at $\vec{f}(\vec{r}, t)$, the ratio between the first two moments:

$$\vec{f}(\vec{r}, t) = \frac{\vec{F}(\vec{r}, t)}{cE(\vec{r}, t)}. \quad (17)$$

For example, in the LP VEF [21, 22]:

$$|\vec{f}(\vec{r}, t)| = \coth(z(\vec{r}, t)) - 1/z(\vec{r}, t) \quad (18)$$

and

$$\chi(\vec{r}, t) = \coth(z(\vec{r}, t))[\coth(z(\vec{r}, t)) - 1/z(\vec{r}, t)]. \quad (19)$$

This VEF is associated with the LP Flux-limiter, (the connection is presented in [21, 22]).

C. Asymptotic Diffusion and asymptotic P_1 (Telegrapher's Equation) Approximations

A common modified version of the diffusion approximation is the asymptotic diffusion approximation [25, 26]. In this approximation, the classic Fick's law (Eq. 8) is replaced by a modified (media-dependent) Fick's law, that

is derived from the exact time-independent asymptotic distribution (in an infinite homogeneous medium, far away from boundaries and strong sources). In this approximation, the classic diffusion coefficient is replaced with a media ($\omega_{\text{eff}}(\vec{r}, t)$ -dependent) diffusion coefficient:

$$D(\vec{r}, t) = \frac{1 - \omega_{\text{eff}}(\vec{r}, t)}{\varkappa_0^2(\vec{r}, t)\sigma_t(T_m(\vec{r}, t))} \equiv \frac{D_0(\vec{r}, t)}{\sigma_t(T_m(\vec{r}, t))} \quad (20)$$

$\varkappa_0(\vec{r}, t)$ is the solution of the transcendental equation, which depends in $\omega_{\text{eff}}(\vec{r}, t)$:

$$\varkappa_0(\vec{r}, t) = \tanh\left(\frac{\varkappa_0(\vec{r}, t)}{\omega_{\text{eff}}(\vec{r}, t)}\right) \quad (21)$$

The numerical values of $\varkappa_0(\omega_{\text{eff}})$ and $D_0(\omega_{\text{eff}})$ were tabulated extensively in [25]. We note that although the asymptotic diffusion approximation produces the correct spatial asymptotic behavior, it still yields infinite particle velocities, missing the correct front (tail) behavior.

In [17, 28], a time-dependent analogy in a P_1 -representation was offered, which is called the asymptotic P_1 approximation. In this approximation, a modified P_1 equation replaces the classic approximated P_1 equation (Eq. 7) with two media-dependent coefficients, $\mathcal{A}(\vec{r}, t)$ and $\mathcal{B}(\vec{r}, t)$:

$$\frac{\mathcal{A}(\vec{r}, t)}{c} \frac{\partial \vec{F}(\vec{r}, t)}{\partial t} + c\vec{\nabla}E(\vec{r}, t) + \mathcal{B}(\vec{r}, t)\sigma_t(T_m(\vec{r}, t))\vec{F}(\vec{r}, t) = 0 \quad (22)$$

$\mathcal{A}(\vec{r}, t)$ and $\mathcal{B}(\vec{r}, t)$ have an explicit form dependent on $\omega_{\text{eff}}(\vec{r}, t)$ [17, 27, 28]. We note that $\mathcal{B}(\vec{r}, t) = 1/D_0(\vec{r}, t)$ ($D_0(\vec{r}, t)$ is the asymptotic diffusion coefficient (Eq. 20)). The full numerical expressions for $\mathcal{A}(\omega_{\text{eff}})$ and $\mathcal{B}(\omega_{\text{eff}})$ are described in Appendix A.

We summarize the setting:

- Using the nominal $\mathcal{A}(\omega_{\text{eff}})$ and $\mathcal{B}(\omega_{\text{eff}})$ is called the asymptotic P_1 approximation (\mathcal{AB} approximation).
- $\mathcal{B}(\omega_{\text{eff}}) = 1/D_0(\omega_{\text{eff}})$ (of Eq. 20) and $\mathcal{A} = 0$ yields the asymptotic diffusion approximation, and hence, we will call it $\mathcal{B}(\vec{r}, t)$ Diffusion approximation (\mathcal{B} approximation).
- $\mathcal{A} = \mathcal{B} = 3$ yields the classic P_1 approximation.
- $\mathcal{B} = 3$ and $\mathcal{A} = 0$ yields the classic diffusion approximation.
- $\mathcal{B} = 3$ and $\mathcal{A} = 1$ yields the *ad hoc* $P_{1/3}$ approximation [15] (In [27], we also offer the asymptotic $P_{1/3}$ approximation, setting $\mathcal{B}(\omega_{\text{eff}}) = 1/D_0(\omega_{\text{eff}})$ and $\mathcal{A} = 1$).

Table I summarizes all the methods itemized above. The results obtained are presented in graphs that will be discussed at a later stage of this paper.

III. THE DISCONTINUOUS ASYMPTOTIC P_1 (TELEGRAPHER'S EQUATION) APPROXIMATION

The asymptotic approximations supplied good descriptions of the transport problem in isotropic media. However, in highly anisotropic media, such as sharp boundaries or strong sources, the asymptotic solutions fail to mirror exactly how the radiation behaves. For example, solving the problem of two adjacent semi-infinite half-spaces (the two-region Milne problem) [30–34], the exact solution is decomposed from an asymptotic part, which tends to the exact solution far from the boundary, and a transient part, which decays relatively fast from the boundary. Actually, this is a generalization of the classic Milne problem [1, 6]. Originally, Milne calculated the angular distribution of the radiated flux from a photosphere of a star. He treated the star as a semi-infinite half-space with a vacuum boundary conditions.

In Fig. 1 we can see a schematic description of the energy density near the boundary between two different regions, based on [38]. Both the asymptotic (solid blue curve) and the transient part (solid red) of the solution are discontinuous, when the exact (solid green) is of course, continuous. The solution (both the asymptotic and transient parts) depends on the properties of the media, via different $\omega_{\text{eff}}(\vec{r}, t)$.

McCormick et. al. solved and tabulated the two-region Milne problem exactly [31–33], defining the exact jump conditions of both the asymptotic scalar flux ($\rho_{2/1} = \phi_{\text{as}}^A/\phi_{\text{as}}^B$) and the current density ($j_{2/1} = J_{\text{as}}^A/J_{\text{as}}^B$), the first two moments, as a function of the $\omega_{\text{eff}}(\vec{r}, t)$ of the two media, ω_{eff}^A and ω_{eff}^B . We note that the two-region Milne problem was solved in many other studies, for example [30, 34]. McCormick et. al. used this tabulation to solve reactor-reflector problems (in a one-dimensional one-group), using a diffusion approximation with these discontinuity (jump) conditions, exactly [29].

Method	In Figures	Basic assumptions
1 IMC Simulation	7,8	Statistical implicit Monte Carlo approach.
2 S_N Simulation	2, 4, 5, 6, 8, 9, 10	Solves the transport equation in N discrete ordinates.
3 Classic Diffusion	2, 4, 5, 6, 7, 8	The specific intensity is a sum of its only two first moments ($\int_{4\pi} I(\hat{\Omega}, \vec{r}, t) \hat{\Omega} \hat{\Omega} d\Omega \approx E(\vec{r}, t)/3$), the derivative of the energy flux $\vec{F}(\vec{r}, t)$ with respect to time inside Eq. 7 is negligible.
4 Classic P_1	2, 4, 5, 6, 7, 8	The specific intensity is a sum of its only two first moments ($\int_{4\pi} I(\hat{\Omega}, \vec{r}, t) \hat{\Omega} \hat{\Omega} d\Omega \approx E(\vec{r}, t)/3$).
5 Larsen Flux limiter	-	General diffusion approximation when the diffusion coefficient is, $D(\vec{r}, t) = \left[(3\sigma_t(T_m(\vec{r}, t)))^n + \left(\frac{1}{E(\vec{r}, t)} \frac{\partial E(\vec{r}, t)}{\partial x} \right)^n \right]^{-1/n}$
6 LP Flux limiter	4, 5, 6	General diffusion approximation when the diffusion coefficient is, $D(\vec{r}, t) = \frac{\lambda(R(\vec{r}, t))}{\omega_{\text{eff}}(\vec{r}, t)}$, $\lambda(R(\vec{r}, t)) = \left[\coth(R(\vec{r}, t)) - \frac{1}{R(\vec{r}, t)} \right] \frac{1}{R(\vec{r}, t)}$, and $R(\vec{r}, t) = \frac{ \vec{\nabla} E(\vec{r}, t) }{\omega_{\text{eff}}(\vec{r}, t) \sigma_t(T_m(\vec{r}, t)) E(\vec{r}, t)}$
7 LP Eddington factor	4, 5, 6	General P_1 approximation when: $\int_{4\pi} I(\hat{\Omega}, \vec{r}, t) \hat{\Omega} \hat{\Omega} d\Omega = \vec{\nabla}(\chi(\vec{r}, t) E(\vec{r}, t))$ $\vec{f}(\vec{r}, t)$, the ratio between the first two moments: $\vec{f}(\vec{r}, t) = \frac{\vec{F}(\vec{r}, t)}{cE(\vec{r}, t)}$. $ \vec{f}(\vec{r}, t) = \coth(z(\vec{r}, t)) - 1/z(\vec{r}, t)$ and $\chi(\vec{r}, t) = \coth(z(\vec{r}, t)) [\coth(z(\vec{r}, t)) - 1/z(\vec{r}, t)]$.
8 Asymptotic diffusion	2	General diffusion approximation, $D(\vec{r}, t) = \frac{1 - \omega_{\text{eff}}(\vec{r}, t)}{\kappa_0^2(\vec{r}, t) \sigma_t(T_m(\vec{r}, t))} \equiv \frac{D_0(\vec{r}, t)}{\sigma_t(T_m(\vec{r}, t))}$ $\kappa_0(\vec{r}, t) = \tanh\left(\frac{\kappa_0(\vec{r}, t)}{\omega_{\text{eff}}(\vec{r}, t)}\right)$
9 Asymptotic P_1	2	P_1 approximation, in \mathcal{AB} form. $\mathcal{B}(\vec{r}, t) = 1/D_0(\omega_{\text{eff}})$

TABLE I. Summary of approximations discussed in Section II.

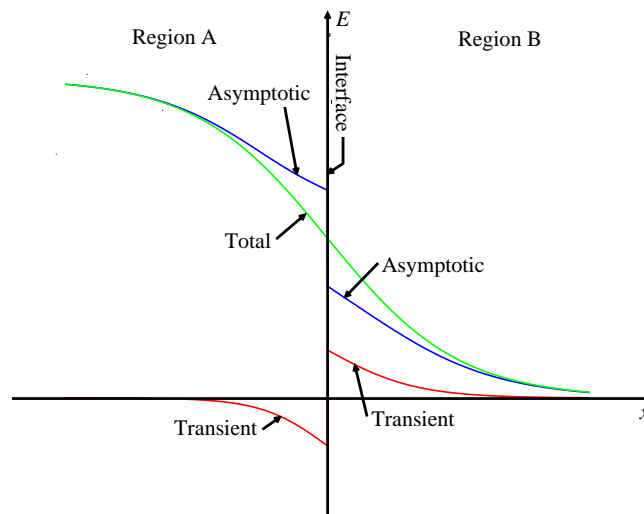


FIG. 1. A schematic description of the energy density near the boundary between different regions, based on [38]. The asymptotic solution is discontinuous (solid blue curve) and tends to the exact solution (green) far from the boundary. The transient part (red) is relevant near the boundary and decay relatively fast far from the boundary.

Zimmerman [35] derived a simple approximation for this two-region boundary problem. In this approximation which is based on a Marshak-like approximation for the exact Milne BC for the two regions problem, the first moment (the energy flux $\vec{F}(\vec{r}, t)$) is continuous, but the zero's moment (the energy density $E(\vec{r}, t)$), is discontinuous. Thus, this approximation conserves particles, and is preferable for time-dependent calculations. Zimmerman expanded this method for deriving a modified discontinuous diffusion approximation. We present a short introduction to this derivation in Sec. III A.

Next, in Sec. III B we will present our analogy for a full time-dependent P_1 asymptotic approximation. In each region, the asymptotic P_1 approximation is valid, and we apply the Zimmerman's discontinuous boundary condition to the energy density. We also generalize this approach for the entire space, deriving the discontinuous asymptotic P_1 equations.

A. The Discontinuous Asymptotic Diffusion Approximation (Zimmerman's $\mu\mathcal{B}$ Approximation)

Using Diffusion (or P_1) approximations, boundary conditions can be satisfied in an integral sense. Zimmerman used the Marshak boundary condition for the incoming flux (when vacuum is a specific case) [35]. In this case, the left and right boundary conditions, located in surface \vec{r}_S [13]:

$$\vec{F}_+(r_S, t) = \int_{\hat{\Omega} \cdot \hat{n} > 0} I(\hat{\Omega}) \hat{\Omega} \cdot \hat{n} d\hat{\Omega} = \frac{\mu(r_S, t)}{2} cE(r_S, t) + \frac{1}{2} \vec{F}(r_S, t) \quad (23a)$$

$$\vec{F}_-(r_S, t) = \int_{\hat{\Omega} \cdot \hat{n} < 0} I(\hat{\Omega}) \hat{\Omega} \cdot \hat{n} d\hat{\Omega} = \frac{\mu(r_S, t)}{2} cE(r_S, t) - \frac{1}{2} \vec{F}(r_S, t) \quad (23b)$$

where \hat{n} is the unit vector perpendicular to the surface, and:

$$\mu(r_S, t) = \begin{cases} \frac{\omega_{\text{eff}}(r_S, t)}{2\kappa_0^2(r_S, t)} \ln \left(\frac{1}{1 - \kappa_0^2(r_S, t)} \right), & \omega_{\text{eff}}(r_S, t) < 1 \\ \frac{\omega_{\text{eff}}(r_S, t)}{2\kappa_0^2(r_S, t)} \ln (1 + \kappa_0^2(r_S, t)), & \omega_{\text{eff}}(r_S, t) > 1 \end{cases} \quad (24)$$

The spatial and temporal dependence of $\mu(\vec{r}, t)$ is due to ω_{eff} , as it is for $\mathcal{A}(\vec{r}, t)$, and $\mathcal{B}(\vec{r}, t)$. The full expression of $\mu(\omega_{\text{eff}})$ is in Appendix A.

Looking at a boundary between two different media (Fig. 1), the flux comes out of medium A, $\vec{F}_-^A(r_S, t)$, is the incoming flux of medium B, $\vec{F}_+^B(r_S, t)$, and vice versa:

$$\vec{F}_+^A(r_S, t) = \vec{F}_-^B(r_S, t) \quad (25a)$$

$$\vec{F}_+^B(r_S, t) = \vec{F}_-^A(r_S, t) \quad (25b)$$

Adding and subtracting Eqs. 25, and using the definitions of Eqs. 23 yield continuous flux ($\vec{F}(r_S, t)$), and thus energy conservation), and a discontinuity in the energy density ($E(r_S, t)$):

$$\vec{F}_A(r_S, t) = \vec{F}_B(r_S, t) \quad (26a)$$

$$\mu_A E_A(r_S, t) = \mu_B E_B(r_S, t) \quad (26b)$$

It can be shown that (assuming the asymptotic diffusion theory is valid far from the boundary) Eqs. 26 yields a modified discontinuous Fick's law [35]:

$$\vec{F}(\vec{r}, t) = -\frac{cD(\vec{r}, t)}{\mu(\vec{r}, t)} \vec{\nabla} (\mu(\vec{r}, t) E(\vec{r}, t)), \quad (27)$$

i.e., Zimmerman extended the discontinuity jump conditions, for an entire non-uniform space. Substituting Eq. 27 in the conservation law, Eq. 5 yields a new discontinuous asymptotic diffusion approximation:

$$\frac{1}{c} \frac{\partial E(\vec{r}, t)}{\partial t} - \vec{\nabla} \cdot \left(\frac{D(\vec{r}, t)}{\mu(\vec{r}, t)} \vec{\nabla} (\mu(\vec{r}, t) E(\vec{r}, t)) \right) = \sigma_a((T_m(\vec{r}, t)) \left(\frac{B(\vec{r}, t)}{c} - E(\vec{r}, t) \right) + \frac{S(\vec{r}, t)}{c} \quad (28)$$

Since Eqs. 27 and 28 contain two medium-dependent variables, $\mu(\omega_{\text{eff}})$ and $D_0(\omega_{\text{eff}})$, we call it the $\mu\mathcal{B}$ approximation (recalling that $\mathcal{B}(\omega_{\text{eff}}) = 1/D_0(\omega_{\text{eff}})$, see Sec. II C).

We note that there are similar works [39, 40], deriving similar discontinuous Fick's law (using $\beta(\omega_{\text{eff}})$ as the discontinuity in the energy density and continuous flux). These works produce, from a different point of view, values close to Zimmerman's $\mu(\omega_{\text{eff}})$. In addition, a discontinuous Fick's law based on the P_2 approximation yields also good results in some neutronics problems [41].

B. Derivation of the Discontinuous Asymptotic P_1 Approximation ($\mu\mathcal{A}\mathcal{B}$ Approximation)

Using the discontinuity jump conditions from the previous section, we can derive a time-dependent analogy, now in a full P_1 form (instead of a Fick's law form in the time-independent case). This approximation contains both $\mathcal{A}(\omega_{\text{eff}})$ and $\mathcal{B}(\omega_{\text{eff}})$ from the asymptotic P_1 approximation, and the jump condition variable $\mu(\omega_{\text{eff}})$, yielding the Discontinuous Asymptotic P_1 Approximation (or in short, the $\mu\mathcal{A}\mathcal{B}$ Approximation).

First, in each region (see Fig. 1) the asymptotic P_1 equations are valid, Eqs. 22 and 5. Suppose that the boundary is located in the origin, i.e. $\vec{r}_S = 0$, we can rewrite Eq. 22 from the two sides of the origin:

$$c \frac{E(\Delta\vec{r}, t) - E(\vec{r}, t)|_{\vec{r} \rightarrow 0+}}{\Delta\vec{r}} = - \frac{\mathcal{A}(\Delta\vec{r}, t)}{c} \frac{\partial \vec{F}(\vec{r}, t)}{\partial t} \Big|_{\vec{r} \rightarrow 0+} - \mathcal{B}(\Delta\vec{r}, t) \sigma_t ((T_m(\Delta\vec{r}, t)) \vec{F}(\vec{r}, t)|_{\vec{r} \rightarrow 0+}) \quad (29a)$$

$$c \frac{E(-\Delta\vec{r}, t) - E(\vec{r}, t)|_{\vec{r} \rightarrow 0-}}{\Delta\vec{r}} = \frac{\mathcal{A}(-\Delta\vec{r}, t)}{c} \frac{\partial \vec{F}(\vec{r}, t)}{\partial t} \Big|_{\vec{r} \rightarrow 0-} + \mathcal{B}(-\Delta\vec{r}, t) \sigma_t ((T_m(-\Delta\vec{r}, t)) \vec{F}(\vec{r}, t)|_{\vec{r} \rightarrow 0-}) \quad (29b)$$

where $E(\vec{r}, t)|_{\vec{r} \rightarrow 0+} = E_B(0, t)$ and $E(\vec{r}, t)|_{\vec{r} \rightarrow 0-} = E_A(0, t)$. $\vec{F}(\vec{r}, t)|_{\vec{r} \rightarrow 0+} = F_B(0, t)$, and $\vec{F}(\vec{r}, t)|_{\vec{r} \rightarrow 0-} = F_A(0, t)$, and their derivatives with respect to time, respectively. Multiplying Eq. 29a by $\mu(\Delta\vec{r}, t) = \mu_B(0, t)$ and Eq. 29b by $\mu(-\Delta\vec{r}, t) = \mu_A(0, t)$, and solving for $E(\vec{r}, t)|_{\vec{r} \rightarrow 0+}$ and $E(\vec{r}, t)|_{\vec{r} \rightarrow 0-}$ yields:

$$c\mu(\Delta\vec{r}, t) \frac{E(\vec{r}, t)|_{\vec{r} \rightarrow 0+}}{\Delta\vec{r}} = c\mu(\Delta\vec{r}, t) \frac{E(\Delta\vec{r}, t)}{\Delta\vec{r}} + \mu(\Delta\vec{r}, t) \mathcal{A}(\Delta\vec{r}, t) \frac{\partial \vec{F}(\vec{r}, t)}{c\partial t} \Big|_{\vec{r} \rightarrow 0+} + \mu(\Delta\vec{r}, t) \mathcal{B}(\Delta\vec{r}, t) \sigma_t ((T_m(\Delta\vec{r}, t)) \vec{F}(\vec{r}, t)|_{\vec{r} \rightarrow 0+}) \quad (30a)$$

$$c\mu(-\Delta\vec{r}, t) \frac{E(\vec{r}, t)|_{\vec{r} \rightarrow 0-}}{\Delta\vec{r}} = c\mu(-\Delta\vec{r}, t) \frac{E(-\Delta\vec{r}, t)}{\Delta\vec{r}} - \mu(-\Delta\vec{r}, t) \mathcal{A}(-\Delta\vec{r}, t) \frac{\partial \vec{F}(\vec{r}, t)}{c\partial t} \Big|_{\vec{r} \rightarrow 0-} - \mu(-\Delta\vec{r}, t) \mathcal{B}(-\Delta\vec{r}, t) \sigma_t ((T_m(-\Delta\vec{r}, t)) \vec{F}(\vec{r}, t)|_{\vec{r} \rightarrow 0-}) \quad (30b)$$

Applying the discontinuity condition in $E(\vec{r}, t)$, Eq. 26(a) and the conservation of flux, Eq. 26(b), and subtracting Eqs. 30 yields:

$$c \frac{\mu(\Delta\vec{r}, t) E(\Delta\vec{r}, t) - \mu(-\Delta\vec{r}, t) E(-\Delta\vec{r}, t)}{2\Delta\vec{r}} + \frac{\mathcal{A}(\Delta\vec{r}, t) \mu(\Delta\vec{r}, t) + \mathcal{A}(-\Delta\vec{r}, t) \mu(-\Delta\vec{r}, t)}{2} \frac{\partial F(\vec{r}, t)}{c\partial t} \Big|_{\vec{r} \rightarrow 0} + \frac{\mu(\Delta\vec{r}, t) \mathcal{B}(\Delta\vec{r}, t) \sigma_t ((T_m(\Delta\vec{r}, t)) \vec{F}(\vec{r}, t)|_{\vec{r} \rightarrow 0}) + \mu(-\Delta\vec{r}, t) \mathcal{B}(-\Delta\vec{r}, t) \sigma_t ((T_m(-\Delta\vec{r}, t)) \vec{F}(\vec{r}, t)|_{\vec{r} \rightarrow 0})}{2} = 0 \quad (31)$$

where $\vec{F}(\vec{r}, t)|_{\vec{r} \rightarrow 0} = \vec{F}(\vec{r}, t)|_{\vec{r} \rightarrow 0+} = \vec{F}(\vec{r}, t)|_{\vec{r} \rightarrow 0-}$ and $\frac{\partial F(\vec{r}, t)}{\partial t} \Big|_{\vec{r} \rightarrow 0} = \frac{\partial F(\vec{r}, t)}{\partial t} \Big|_{\vec{r} \rightarrow 0+} = \frac{\partial F(\vec{r}, t)}{\partial t} \Big|_{\vec{r} \rightarrow 0-}$ from Eq. 26a, of course. Taking $\Delta\vec{r} \rightarrow 0$ yields a general discontinuous asymptotic P_1 equation (for the entire space):

$$\mu(\vec{r}, t) \frac{\mathcal{A}(\vec{r}, t)}{c} \frac{\partial F(\vec{r}, t)}{\partial t} + c\vec{\nabla} \cdot (\mu(\vec{r}, t) E(\vec{r}, t)) + \mu(\vec{r}, t) \mathcal{B}(\vec{r}, t) \sigma_t ((T_m(\vec{r}, t)) F(\vec{r}, t)) = 0 \quad (32)$$

Eqs. 5 and 32 define the new approximation, the *discontinuous asymptotic P_1 approximation*. These equations contain three medium-dependent variables, $\mu(\omega_{\text{eff}})$ and $\mathcal{A}(\omega_{\text{eff}})$ and $\mathcal{B}(\omega_{\text{eff}})$, and thus we call it also the $\mu\mathcal{A}\mathcal{B}$ approximation. Our new approximation has the advantage of the P_1 notation along with the using of the asymptotic exact solutions. It is also important to note the method reserves energy which is important for the physical meaning.

The discontinuous asymptotic P_1 approximation is valid also for neutronics, replacing $E(\vec{r}, t)$ and $\vec{F}(\vec{r}, t)$ with $\phi(\vec{r}, t)$ and $\vec{J}(\vec{r}, t)$ and ω_{eff} with c (do not confuse with the speed of light). For a more detailed discussion, see Appendix B. Also, the extension to multi-group is straightforward due to the energy dependent definition of ω_{eff} (or c , in the case of neutronics) [18, 24].

By assuming that both the time derivative of $\vec{F}(\vec{r}, t)$ and the spatial derivative of $\mathcal{A}/\mathcal{B}\sigma_t$ are small enough, we can neglect $\vec{\nabla} \left(\frac{\mathcal{A}(\vec{r}, t)}{\mathcal{B}(\vec{r}, t)\sigma_t(T_m(\vec{r}, t))} \right) \cdot \frac{\partial \vec{F}(\vec{r}, t)}{\partial t}$ and obtained from Eqs. 32 and 5:

$$\begin{aligned} & \frac{\mathcal{A}(\vec{r}, t)}{\mathcal{B}(\vec{r}, t)c\sigma_t} \frac{\partial^2 E(\vec{r}, t)}{\partial t^2} - \vec{\nabla} \left[\frac{c}{\sigma_t \mu(\vec{r}, t) \mathcal{B}(\vec{r}, t)} \vec{\nabla} (\mu(\vec{r}, t) E(\vec{r}, t)) \right] + \frac{\partial E(\vec{r}, t)}{\partial t} = \\ & \frac{4\pi \mathcal{A}(\vec{r}, t)}{c \mathcal{B}(\vec{r}, t) \sigma_t} \frac{\partial (\sigma_a B(\vec{r}, t))}{\partial t} - \frac{\mathcal{A}(\vec{r}, t)}{\mathcal{B}(\vec{r}, t) \sigma_t} \frac{\partial (\sigma_a E)}{\partial t} + \\ & \frac{\mathcal{A}(\vec{r}, t)}{\mathcal{B}(\vec{r}, t) \sigma_t} \frac{\partial S(\vec{r}, t)}{\partial t} + \sigma_a (4\pi B(\vec{r}, t) - cE(\vec{r}, t)) + S(\vec{r}, t) \end{aligned} \quad (33)$$

This is the *discontinuous asymptotic Telegrapher's equation* which is our new modification of Eq. 10.

IV. RESULTS

In this section we test the new discontinuous asymptotic P_1 approximation ($\mu\mathcal{A}\mathcal{B}$ approximation) numerically, with some well-known radiative transfer benchmarks. The numerical results are compared to exact benchmarks' solutions, as well as other approximations that were introduced in Sec. II. The first benchmark is the well-known constant opacity Su-Olson benchmark [36]; the other is a variable non-linear opacity Olson's benchmark [15]. We will see that the new method seems to be more accurate than other methods, while still being easy to apply.

A. The Constant Opacity (Su-Olson) problem

The well-known Su-Olson benchmark [36] is a basic non-equilibrium slab-geometry radiative transfer benchmark that uses a constant opacity in an infinite, isotropic scattering medium. The radiation source in the medium is isotropic and constant for a limited period (and is zero afterwards) and the material is initially cold and homogeneous. In this benchmark it is convenient to set dimensionless position z and time τ , and normalized radiation and material energy densities, W and V , respectively:

$$x = \sigma_t z; \quad \tau = \epsilon c \sigma_t t; \quad V = \left(\frac{T}{T_H} \right)^4; \quad W = \int_{-1}^1 d\mu \frac{I(\mu)}{a T_H^4}; \quad (34)$$

T_H is defined as the Hohlraum temperature (or any other reference temperature). The material heat capacity is defined as: $C_v = \alpha T^3$ and $\epsilon = 4a/\alpha$. It is also convenient to define the ratio of the scattering cross section to the total cross section $c_s = \sigma_s/\sigma_t$, since we use dimensionless position variable. This problem has an exact solution [36] for a specific source term $S(x, \tau)$:

$$S(x, \tau) = \begin{cases} 1, & \text{if } \tau \leq 10, \quad x \leq 0.5 \\ 0, & \text{otherwise} \end{cases} \quad (35)$$

The radiation energy as a function of space is presented in Fig. 2 using several approximations and the exact solution for the no scattering case, $c_s = 0$. In Fig. 2(a) the radiation energy is shown in linear scale for $\tau = 3.16$, and in Fig. 2(b) in logarithmic scale for $\tau = 1$. We note that for the non-scattering case ($c_s = 0$), there is an analytic solution for the classic P_1 approximation [42], and our numerical results reproduce this analytic solution.

First, the benchmark results (full symbols) and S_{32} numerical solutions (green solid curves) fit perfectly. Next, both the classic diffusion and P_1 approximations (dashed and solid curves) yield bulk energy results that are too low. (Fig. 2(a)). In addition, in the logarithmic scale (Fig. 2(b)) it is noticeable that the diffusion approximation heat front is too fast, while P_1 heat front is too slow. The asymptotic diffusion approximation (blue dash curves) suffers from the same problems, yielding just a little bit better results than the classic diffusion approximation. The front of the asymptotic P_1 (blue solid curves), is quite good but has too small bulk energy, and is similar to the classic P_1 approximation. Zimmerman's discontinuous asymptotic diffusion approximation (the $\mu\mathcal{B}$ approximation),

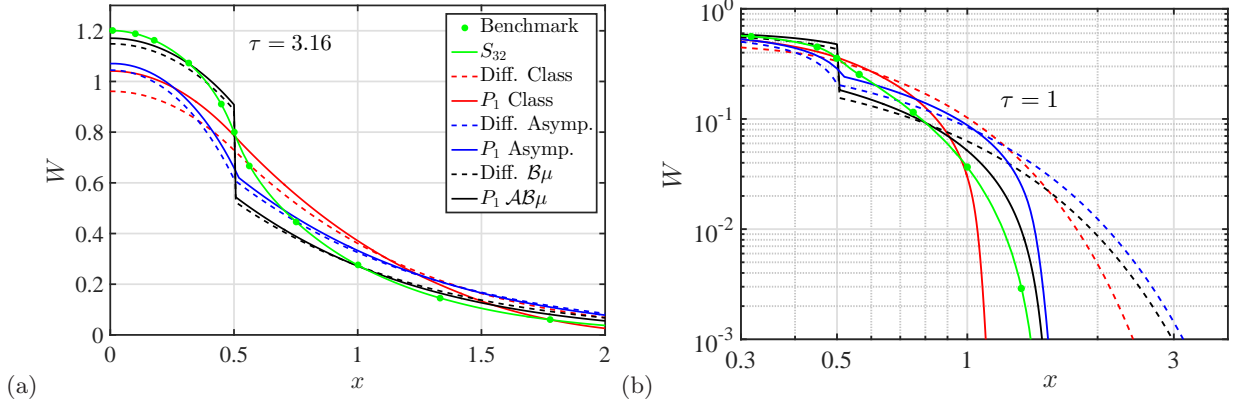


FIG. 2. The radiation energy density (W) in linear (a) and logarithmic (b) scales as a function of the optical depth. The Su-Olson problem here is for a non scattering case, $c_s = 0$. The circles are the exact transport solution which is taken from [36], the green curves are the S_{32} . The red dashed and solid curves are the classic diffusion and P_1 approximations, respectively. The blue dashed and solid curves are the asymptotic diffusion and P_1 approximations. The black dashed and solid curves are Zimmerman's $B\mu$ diffusion and the $\mathcal{AB}\mu$ P_1 approximations.

yields better results in the bulk, resulting the discontinuity jump condition, but the front is still too fast, as any diffusion approximation (because of the infinite velocity). However, it is clear that the new discontinuous asymptotic P_1 approximation (the $\mu\mathcal{AB}$ approximation) is very close to the exact solution, both in the bulk and the front (except the jump itself).

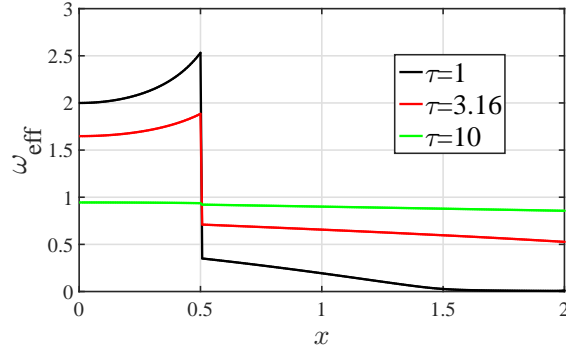


FIG. 3. The ω_{eff} for our $\mathcal{AB}\mu$ approximation. Here ω_{eff} is for three different times, $\tau = 1, 3.16, 10$. The jump in $x = 0.5$ is due to the step function in the source term.

Of course, in the interface of the source (in $x = 0.5$), there is a large discontinuity in the energy density (both employ the new approximation or Zimmerman's approximation). This is due to the functional dependence of $\mu(x, \tau)$ on $\omega_{\text{eff}}(x, \tau)$ (Eq. 24). which is a function of time and space. In Fig. 3 we can see $\omega_{\text{eff}}(x, \tau)$ as a function of x for several times. The clear jump in $x = 0.5$ is due to the step function of $S(x, \tau)$ (Eq. 35), and it is mostly important in early times. As the energy increases in later times, $S(x, \tau)$ is less important in the ω_{eff} , and the discontinuity is less apparent.

Moreover, the new $\mu\mathcal{AB}$ approximation yields better results than the gradient-dependent approximations, such as the different Flux-Limiters and variable Eddington factors approximations. In Fig. 4 (blue dashed and solid curves) we introduce the results of the Levermore-Pomraning flux limiter and Eddington factor. We found that it yields better or similar results than other flux-limiters or Eddington factors, such as Minerbo's or Kershaw's (see also in [15, 16]). The LP FL results are quite similar to the LP VEF results, when the latter yields slightly better results. We can see that the new $\mu\mathcal{AB}$ approximation yields better results than these gradient-dependent approximations. This is extremely important since the gradient-dependent approximations are harder to apply in multi-dimensions (especially in curvilinear geometries), while the new approximation is easy to apply as a simple P_1 implementation.

In Fig. 5 we can see the material energy for the case of $c_s = 0$. We can see that the same conclusions that were presented regarding the radiation energy, are also valid for the material energy. The new $\mu\mathcal{AB}$ approximation yields the best estimations compared to the exact results (except the jump itself, that is of course, non-physical). In Fig. 6

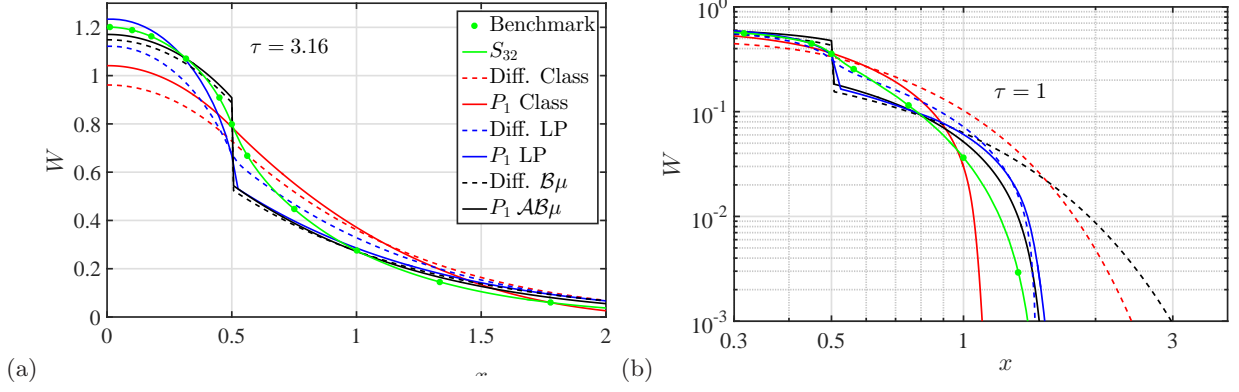


FIG. 4. The Su-Olson benchmark radiation energy (W) with $c_s = 0$ in linear scale (a) and in logarithmic scale (b). In addition to the exact results, classic diffusion and P_1 approximations and the discontinuous approximations as in Fig. 2, the Levermore-Pomraning FL (dashed blue curves) and the Levermore-Pomraning VEF (solid blue curves) are presented.

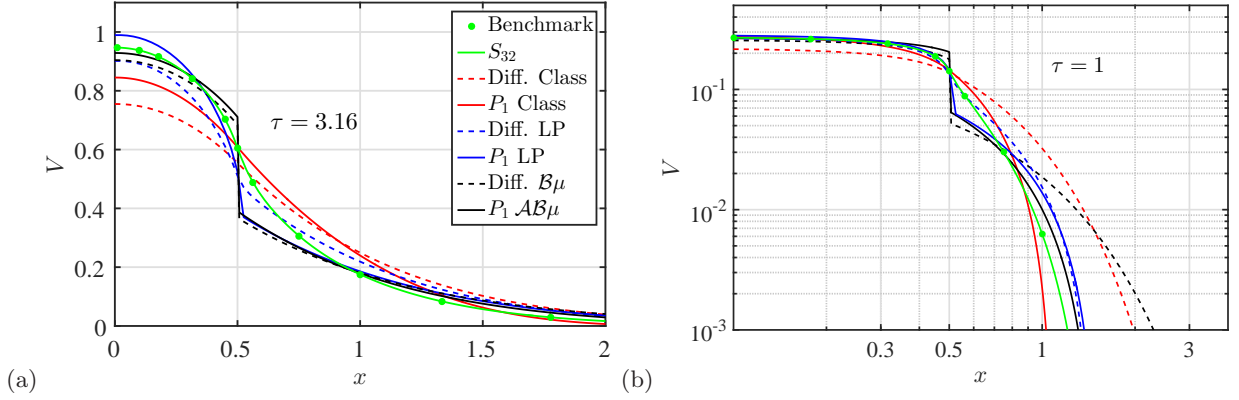


FIG. 5. The same as Fig. 4 but for the material energy V .

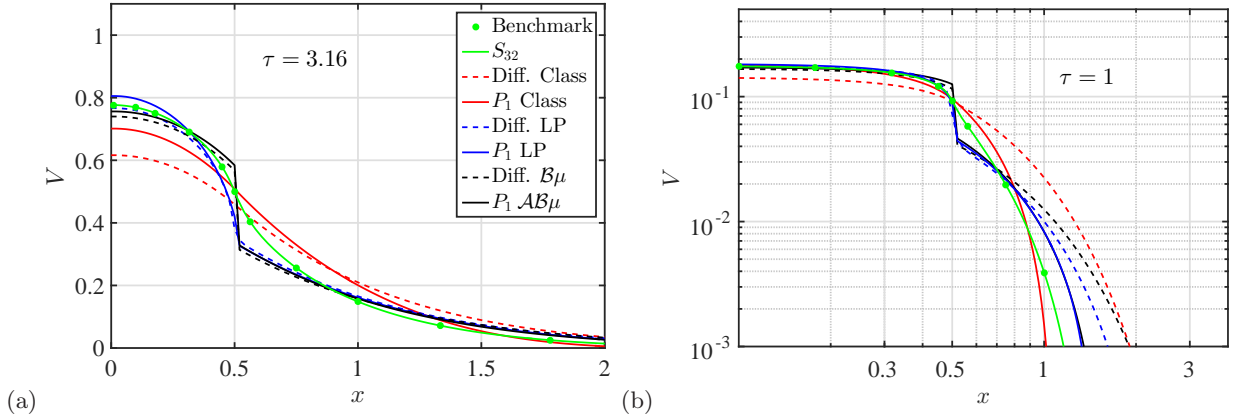


FIG. 6. The same as Fig. 5 but for the scattering-included case, $c_s = 0.5$.

we can see that the same is also valid for scattering media with $c_s = 0.5$ as well (we present here the material energy since the radiation energy is very close to the $c_s = 0$ case, Fig. 4). The discontinuity jump in the $c_s = 0.5$ case is smaller than in the $c_s = 0$ case, due to smaller differences in ω_{eff} in the scattering-included case.

B. Olson's non-linear opacity problem

The assumption of constant opacity which allows the semi-analytic solution that is made in the Su-Olson is usually, not realistic, since the opacity is a strong function of the material temperature. Therefore, Olson [15] set another benchmark, where the opacity varies with the material temperature:

$$\sigma_a = T^{-3} \quad (36)$$

In this problem, C_v is constant and the dimensionless time τ is:

$$\tau = \frac{4acT_H^3 t}{C_v} \quad (37)$$

We note that the T^{-3} dependence is quite realistic opacity for low-Z materials such as Aluminum [43]. Instead of an internal source term (like in the Su-Olson benchmark), Olson et. al. apply an isotropic incident radiation flux located on the slab's surface at $x = 0$:

$$F_{in} = \frac{acT_H^4}{4} \quad (38)$$

Applying the Marshak boundary condition and solving for the net flux $F(0, \tau)$ [15]:

$$F(x=0, \tau) = \begin{cases} \text{Classic } P_1/\text{Diffusion,} & 2F_{in} - cW(0, \tau)/2 \\ \text{Asymptotic } P_1/\text{Diffusion,} & 2F_{in} - \mu(0, \tau)cW(0, \tau) \end{cases} \quad (39)$$

when $\mu(0, \tau)$ is a function of $\omega_{\text{eff}}(0, \tau)$ as defined by Eq. 24, assuming the asymptotic flux distribution instead of the classic P_1 notation [13].

First we solve this problem with two exact approximations, both S_N with $N = 32$ and Implicit Monte Carlo (IMC) [14]. Both methods yield precisely the same solution, so we choose to introduce explicitly here the IMC results. The results of the Olson's nonlinear opacity benchmark are shown in Fig. 7. In Fig. 7(a) we introduce the difference between the radiation and material temperatures. The results (of both S_N and IMC) are very similar to the exact VEF that was introduced in [15]. Since in this benchmark $T_H = 1$, the problem turned out to be relatively thick in optical terms, when there exists a large number of mean free paths even at early times. That is why the material temperature (T_m) is very close to the radiation temperature (T_r). In Fig. 7(b), we present the radiation temperature (as obtained by different approximations), versus the exact solution. We can see that all approximation are bunched close to the IMC due to the fact that $T_H = 1$ yields an optically thick problem.

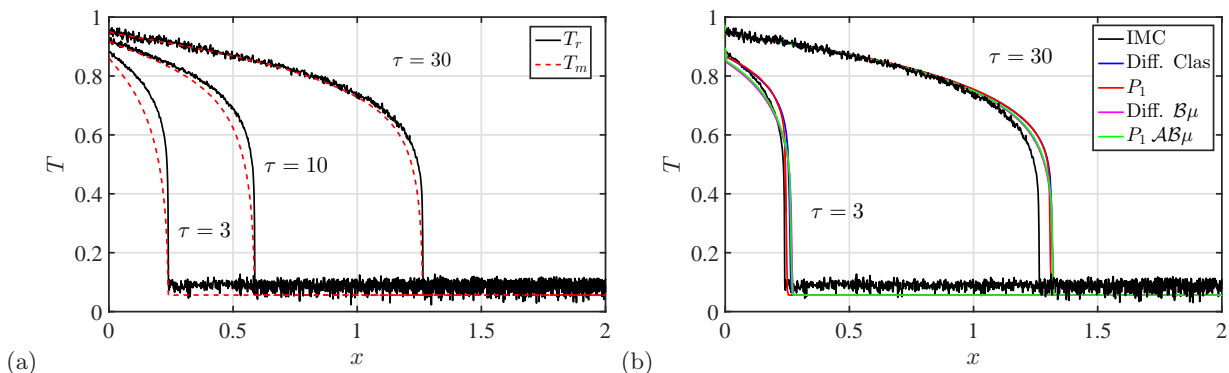


FIG. 7. (a) The radiation and material temperatures of the IMC in different times ($\tau = 3, 10, 30$) for the Olson's nonlinear opacity problem (using $T_H = 1$). (b) The radiation temperature (T_r), as a function of the optical depth in different times ($\tau = 3, 30$). The red and blue solid curves are the classic diffusion and P_1 . The magenta and the green curves are the $\mathcal{B}\mu$ diffusion and the $\mathcal{A}\mathcal{B}\mu P_1$ approximations. The exact IMC is in the black solid curves.

Thus, we offer an Olson's-like optically thin benchmark, by increasing the incoming flux and set $T_H = 5$ (and thus, $F_{in} = \frac{5acT_H^4}{4}$). Since the opacity of the problem depends as T_m^{-3} with the material temperature (Eq. 36), the opacity decreases significantly. In Fig. 8 the results of the Olson-like nonlinear opacity benchmark using $T_H = 5$ are shown. We can see in Fig. 8(a) that the difference between the radiation and material temperatures in different

times increases in comparison with $T_H = 1$ case. Moreover, In Fig. 8(b) we introduce the radiation temperature using several approximations and the exact (IMC) solution. We can see that the P_1 (red solid curve) is too slow, and both the classic and Zimmerman's $\mu\mathcal{B}$ diffusion approximations (blue and magenta solid curved) propagate too fast. The new $\mu\mathcal{AB}$ approximation yields quite close results to the exact solutions, obtaining almost the correct heat front.

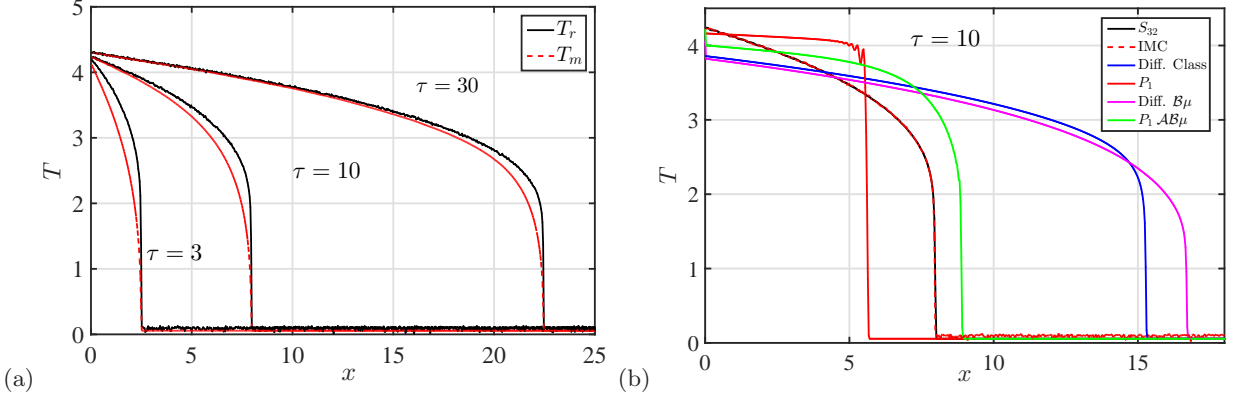


FIG. 8. (a) The radiation and material temperatures of the IMC in different times ($\tau=3, 10, 30$) for the Olson's-like problem using $T_H = 5$. (b) The the radiation temperature (T_r), as a function of the optical depth in $\tau = 10$. The red and blue solid curves are the classic diffusion and P_1 . The magenta and the green curves are the $\mathcal{B}\mu$ diffusion and the $\mathcal{AB}\mu P_1$ approximations, respectively. The exact IMC is the black solid curves.

V. ENERGY DENSITY AND FLUX DISCONTINUITY ($\alpha\beta\mathcal{B}$ AND $\alpha\beta\mathcal{AB}$ APPROXIMATIONS)

In Sec. III we have introduced the two-region Milne problem, indicating that both the asymptotic energy density and flux are discontinuous. In Sec. III A we noted that Zimmerman offered a Marshak-like approximation for the jump conditions that have discontinuity in the energy density but have a continuous flux (and thus, conserves particles). Next, in Sec. III B we introduced the new $\mu\mathcal{AB}$ approximation that uses Zimmerman's Marshak-like approximate jump conditions to derive a modified discontinuous asymptotic P_1 approximation. The question we now wish to pose is whether we can go further and employ the precise Milne jump conditions to derive an even more accurate approximation.

First, McCormick et. al. solved the exact two-region problem, finding the discontinuous jump conditions of the energy density ($\rho_{2/1} = E_{\text{as}}^A/E_{\text{as}}^B$) and the flux ($j_{2/1} = \vec{F}_{\text{as}}^A/\vec{F}_{\text{as}}^B$) [31, 32]. both $\rho_{2/1}$ and $j_{2/1}$ are functions of the $\omega_{\text{eff}}(\vec{r}, t)$ of the two media, ω_{eff}^A and ω_{eff}^B . McCormick at al. have also fully tabulated the numerical values of $\rho_{2/1}$ and $j_{2/1}$ [33]. We note that the exact solution of the two-region problem was introduced in many other papers, for example in [34]. A minor approximation, based on variational analysis yields very close values of the discontinuities, by introducing the discontinuities in both energy density and radiation flux as [34, 44]:

$$\beta_A(\vec{r}_S, t)E_A(\vec{r}_S, t) = \beta_B(\vec{r}_S, t)E_B(\vec{r}_S, t) \quad (40a)$$

$$\alpha_A(\vec{r}_S, t)\vec{F}_A(\vec{r}_S, t) = \alpha_B(\vec{r}_S, t)\vec{F}_B(\vec{r}_S, t) \quad (40b)$$

The dependence of $\alpha(\vec{r}_S, t)$ and $\beta(\vec{r}_S, t)$ in space and time is again due to ω_{eff} (see Appendix A). This form of applying the discontinuous condition is more convenient to apply in numerical codes, setting $\rho_{2/1} = \beta(\omega_{\text{eff}}^B)/\beta(\omega_{\text{eff}}^A)$ and $j_{2/1} = \alpha(\omega_{\text{eff}}^B)/\alpha(\omega_{\text{eff}}^A)$, and the difference from the exact solution is minor (for an accuracy check comparing to the exact McCormick solutions, see Appendix C).

Following the procedure described in Zimmerman's discontinuous diffusion (Sec. III A), Eqs. 40 yields modified P_1 equations (see in [34, 44] for the time-independent case):

$$\frac{1}{c} \frac{\partial E(\vec{r}, t)}{\partial t} + \frac{1}{c\alpha(\vec{r}, t)} \nabla \cdot (\alpha(\vec{r}, t)\vec{F}(\vec{r}, t)) = \sigma_a(T_m(\vec{r}, t)) \left(\int_{4\pi} \frac{B(\vec{r}, t)}{c} - E(\vec{r}, t) \right) + \frac{S(\vec{r}, t)}{c} \quad (41a)$$

$$\vec{F}(\vec{r}, t) = -\frac{cD(\vec{r}, t)}{\beta(\vec{r}, t)} \vec{\nabla} (\beta(\vec{r}, t)E(\vec{r}, t)), \quad (41b)$$

Eq. 41a replaces the conservation law (Eq. 5), and thus *does not* conserve particles (the conserved quantity is $\alpha(\vec{r}, t)\vec{F}(\vec{r}, t)$ instead), which makes it less favorable. Eq. 41b is identical to Eq. 27, replacing $\beta(\omega_{\text{eff}})$ with $\mu(\omega_{\text{eff}})$. Eqs. 41 yields a discontinuous asymptotic diffusion, that does not conserve particles. By recalling that $\mathcal{B}(\omega_{\text{eff}}) = 1/D_0(\omega_{\text{eff}})$, this diffusion approximation is called the $\alpha\beta\mathcal{B}$ approximation.

Next, in a similar way to the derivation of the new $\mu\mathcal{A}\mathcal{B}$ approximation (see Sec. III B), we can derive a modified $\alpha\beta\mathcal{A}\mathcal{B}$ P_1 equation, Eq. 41a and:

$$\beta(\vec{r}, t) \frac{\mathcal{A}(\vec{r}, t)}{c} \frac{\partial F(\vec{r}, t)}{\partial t} + c\vec{\nabla} \cdot (\beta(\vec{r}, t)E(\vec{r}, t)) + \beta(\vec{r}, t)\mathcal{B}(\vec{r}, t)\sigma_t((T_m(\vec{r}, t))F(\vec{r}, t)) = 0 \quad (42)$$

which is identical to Eq. 32, replacing $\beta(\omega_{\text{eff}})$ with $\mu(\omega_{\text{eff}})$. Eqs. 41a and 42 are thus the $\alpha\beta\mathcal{A}\mathcal{B}$ approximation.

The results of the Su-Olson constant opacity benchmark using this $\alpha\beta\mathcal{A}\mathcal{B}$ approximation (in discontinuous P_1 notation) and the $\alpha\beta\mathcal{B}$ approximation (in discontinuous diffusion notation) are presented in Fig. 9 for $c_s = 0$, and in Fig. 10 for $c_s = 0.5$.

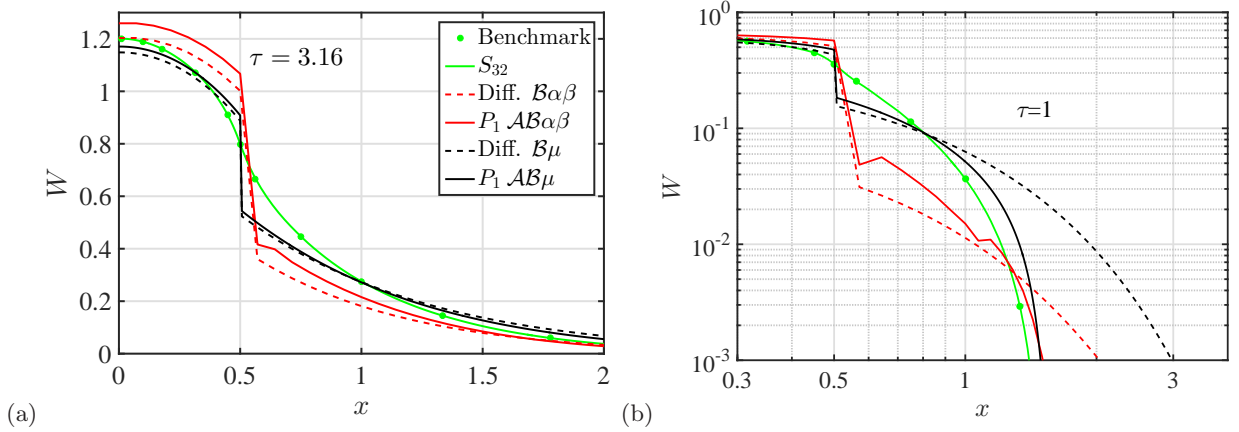


FIG. 9. The radiation energy density (W) in linear (a) and logarithmic (b) scales as function of space in different times, for the case of $c_s = 0$. The exact transport solution is in The circles are where the S_{32} are represented by the green curves. The red dashed and solid curves are the $\alpha\beta\mathcal{B}$ discontinuous diffusion and the $\mathcal{A}\mathcal{B}\alpha\beta$ discontinuous P_1 approximations. The blue solid and dashed curves are the $\mathcal{B}\mu$ discontinuous diffusion and $\mathcal{A}\mathcal{B}\mu$ discontinuous P_1 approximations.

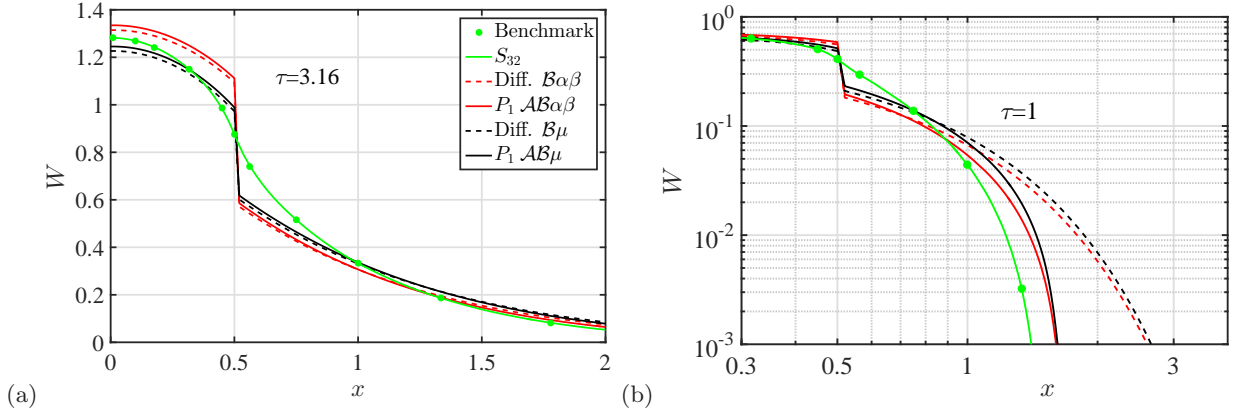


FIG. 10. The same as Fig. 9 for the scattering-included case, $c_s = 0.5$.

First, it turns out that using $\alpha(\omega_{\text{eff}})$ and $\beta(\omega_{\text{eff}})$ instead of $\mu(\omega_{\text{eff}})$, causes essential numerical difficulties, especially in the purely absorbing case (which is the most common physical case; scattering is usually negligible). The noisy results can be seen in the purely absorbing case in Fig. 9, and the numerical scheme is often unstable. This is due to the fact that $\alpha(\omega_{\text{eff}})$ and $\beta(\omega_{\text{eff}})$ both go to infinity when $\omega_{\text{eff}} \rightarrow 0$ [34, 44]. In the scattering-included case, $c_s = 0.5$, the results are much smoother as can be seen in Fig. 10, since the scattering prevents the $\omega_{\text{eff}} \rightarrow 0$ limit. We note again, as is the case in any diffusion approximation, the $\alpha\beta\mathcal{B}$ approximation yields a heat front that is too fast. When

the approximations are stable (such as the scattering-included case), the results have similar (or less) accuracy as the new $\mu\mathcal{AB}$ approximation.

In conclusion, since the fact that in many cases this approximation is numerically unstable, and when the solution is available the accuracy is similar to (or even less than) the stable $\mu\mathcal{AB}$ approximations, we *do not* recommend using $\alpha\beta\mathcal{AB}$ or $\alpha\beta\mathcal{B}$ approximations (at least in radiative transfer problems).

VI. DISCUSSION

In this paper we have derived a new approximate method for solving the mono-energetic gray transport equation, the discontinuous asymptotic P_1 approximation (or the $\mu\mathcal{AB}$ approximation). This method rests on two foundations: The asymptotic P_1 approximation [17], that reproduces the asymptotic steady-state behavior and prevents the infinite particle velocities (unlike the diffusion approximations), and the discontinuity jump conditions of Zimmerman's discontinuous diffusion [35], forcing a discontinuity in the energy density and continuous flux (and thus, conserves particles).

We show that this approximation yields better results than do other common methods in two important benchmark problems, the Su-Olson constant opacity benchmark (both with or without scattering) [36] and Olson's non-linear opacity (temperature-dependent) problem [15]. The new approximation yields even better results than the gradient-dependent approximations, such as various Flux-Limiter approximations or the variable Eddington factor approximations. We consider this method to be better grounded in physics than others, in that it relies on precise asymptotic solutions, which are indeed discontinuous. That may explain the quality of its results.

We have also tested the possibility for using a method that includes discontinuities in both energy density and radiation flux (the $\alpha\beta\mathcal{AB}$ approximation), based on the exact two-region Milne problem. We have found that these methods often suffer from numerical instabilities, while when stable the accuracy is similar to the $\mu\mathcal{AB}$ approximation. Due to these observations, and the fact that this approximation does not conserve particles, we conclude that the $\mu\mathcal{AB}$ approximation is preferable.

In future work, we plan to test the new approximation against actual supersonic Marshak-wave experiments [7, 8], comparing it to exact approaches such as S_N or IMC. In addition, it would be interesting to test the new approximation in 2D/3D. The new method depends explicitly *only* on ω_{eff} , when ω_{eff} is defined on the middle of the numerical cell, just like E . In gradient-dependent approximations such as the VEF or FL, the approximation depends on \vec{F}/E , where \vec{F} is defined on cell edges, which makes it much more complicated to solve in multi-dimensional scheme

This numerical advantage of the new scheme will become very important if it can be extended to higher dimensions.

Appendix A: Numerical Values For $\mathcal{A}(\omega_{\text{eff}})$, $\mathcal{B}(\omega_{\text{eff}})$ and $\mu(\omega_{\text{eff}})$

Here we introduce full numerical expressions that were used for the ω -dependent functions (For simplicity, we set here $\omega_{\text{eff}} \equiv \omega$): We recall that $\mathcal{B}(\omega)$ in Eq. 22 is equal to $= 1/D_0(\omega)$ from Eq. 20. $\mathcal{A}(\omega)$ and $\mathcal{B}(\omega)$ were taken as was explained in [17, 27, 28]:

$$\mathcal{A}(\omega) = \begin{cases} 0.96835 - 0.437\omega, & \text{if } 0.55 \leq \omega \leq 0.65 \\ \frac{0.247(0.433+0.421\omega-2.681\omega^2-1.82\omega^3+4.9\omega^4-1.06\omega^5+2.56\omega^6)}{(0.33+0.159\omega-0.567\omega^2-\omega^3)^2}, & \text{otherwise} \end{cases} \quad (\text{A1})$$

$$\mathcal{B}(\omega) = \begin{cases} \frac{1}{0.80054-0.523\omega}, & \text{if } 0.59 \leq \omega \leq 0.61 \\ \frac{0.1326495+\omega[0.03424169+\omega(0.1774006-\omega)]}{0.3267567+\omega[0.1587312-\omega(0.5665676+\omega)]} \cdot \frac{1+\omega}{0.40528473}, & \text{otherwise} \end{cases} \quad (\text{A2})$$

Calculating the third ω -dependent function, $\mu(\omega)$ as was defined in Eq. 24 is through the definition of $\kappa(\omega)$, the solution of the transcendental Eq. 21. A numerical evaluation of $\kappa(\omega)$ can be [25]:

$$\kappa^2(\omega) = \begin{cases} 1, & \omega < 0.01 \\ 1 - 4e^{-\frac{2}{\omega}} \left(1 + \frac{4-2\omega}{\omega} e^{-\frac{2}{\omega}} + \frac{24+20\omega+3\omega^2}{\omega^2} e^{-\frac{4}{\omega}} \right), & 0.01 < \omega \leq 0.45 \\ (1-\omega)\mathcal{B}(\omega), & 0.45 < \omega < 1 \\ (\omega-1)\mathcal{B}(\omega), & \omega \geq 1 \end{cases} \quad (\text{A3})$$

Subsequently, $\mu(\omega)$ itself is calculated [35]:

$$\mu(\omega) = \begin{cases} 1, & \omega < 0.01 \\ -\frac{\omega}{2\kappa^2(\omega)} \log(1 - \kappa^2(\omega)), & \kappa^2(\omega) > 0 \\ 1, & \text{otherwise} \end{cases}, \quad \begin{matrix} \omega < 0.01 \\ 0.01 \leq \omega < 0.999 \\ 0.999 \leq \omega \leq 1.001 \\ \omega > 1.001 \end{matrix} \quad (\text{A4})$$

$\alpha(\omega)$ and $\beta(\omega)$ from Eqs. 40, were calculated in a manner similar to that suggested in [44] (Eqs. 95-96) or in [34] (Eqs. 77-78). In Fig. 11 we introduce the curves of $\mu(\omega)$, $\beta(\omega)$ and $\alpha(\omega)$. We can see that both $\beta(\omega)$ and $\alpha(\omega)$ go to infinity when $\omega \rightarrow 0$, causing numerical instabilities on the $\alpha\beta$ -included approximations. Similar figures for $\mathcal{A}(\omega)$ and $\mathcal{B}(\omega)$ may be found in [17, 27, 28].

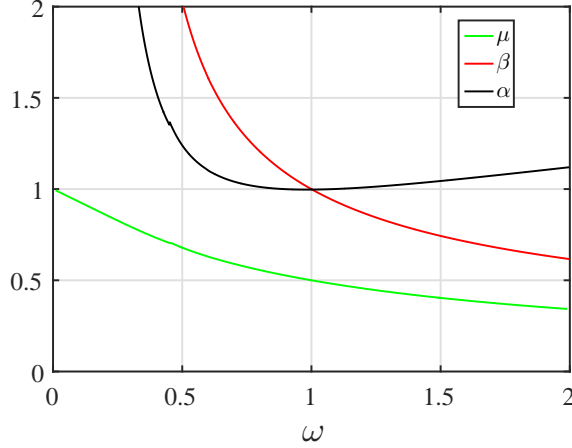


FIG. 11. The functions $\mu(\omega)$, $\beta(\omega)$ and $\alpha(\omega)$. $\beta(\omega)$ and $\alpha(\omega)$ goes to infinity when $\omega \rightarrow 0$.

Appendix B: The Discontinuous Asymptotic P_1 Approximation for Neutronics

In neutronics, the mono-energetic Boltzmann equation is (equivalent to Eq. 1 in this work) [28]:

$$\frac{1}{v} \frac{\partial \psi(\hat{\Omega}, \vec{r}, t)}{\partial t} + \hat{\Omega} \cdot \vec{\nabla} \psi(\hat{\Omega}, \vec{r}, t) + \Sigma_t(\vec{r}) \psi(\hat{\Omega}, \vec{r}, t) = \int_{4\pi} d\hat{\Omega}' \Sigma_s(\hat{\Omega} \cdot \hat{\Omega}', \vec{r}) \psi(\hat{\Omega}', \vec{r}, t) + \nu(\vec{r}) \Sigma_f(\vec{r}) \int_{4\pi} d\hat{\Omega}' \psi(\hat{\Omega}', \vec{r}, t) + S(\hat{\Omega}, \vec{r}, t) \quad (\text{B1})$$

when $\psi(\hat{\Omega}, \vec{r}, t)$ is the angular flux. $\Sigma_t(\vec{r}) = \Sigma_a(\vec{r}) + \Sigma_s(\vec{r}) + \Sigma_f(\vec{r})$ is the total cross-section when $\Sigma_a(\vec{r})$ is the absorbing cross-section, $\Sigma_s(\vec{r}) \equiv \int_{-1}^1 d\mu_0 \Sigma_s(\mu_0, \vec{r})$ is the scattering cross-section ($\mu_0 \equiv \hat{\Omega} \cdot \hat{\Omega}'$) and $\Sigma_f(\vec{r})$ is the fission cross-section. $S(\hat{\Omega}, \vec{r}, t)$ is an external source term, $\nu(\vec{r})$ is the mean number of neutrons that are emitted per fission and v is the neutron velocity. Here we use the scalar flux $\phi(t, \vec{r})$ and the total current $\vec{J}(t, \vec{r})$ as the first two moments of $\psi(\hat{\Omega}, \vec{r}, t)$ (equivalent to $E(\vec{r}, t)$ and $\vec{F}(\vec{r}, t)$ in this work), while $c(t, \vec{r})$ (which is called *the albedo*), the mean number of particles emitted from a collision, is replacing $\omega_{\text{eff}}(t, \vec{r})$, and is defined as:

$$c(\vec{r}, t) = \frac{\Sigma_s(\vec{r}) + \nu(\vec{r}) \Sigma_f(\vec{r}) + S(t, \vec{r}) / (v \Sigma_t(\vec{r}) \phi(t, \vec{r}))}{\Sigma_t(\vec{r})} \quad (\text{B2})$$

The first P_1 equation, the conservation law for neutronics is (equivalent to Eq. 5):

$$\frac{1}{v} \frac{\partial \phi(t, \vec{r})}{\partial t} + \vec{\nabla} \cdot \vec{J}(t, \vec{r}) + \Sigma_a(\vec{r}) \phi(t, \vec{r}) = (\nu(\vec{r}) - 1) \Sigma_f(\vec{r}) \phi(t, \vec{r}) + S(t, \vec{r}), \quad (\text{B3})$$

and the equivalent to the second discontinuous asymptotic P_1 equation, Eq. 32, is:

$$\mu(\vec{r}, t) \frac{\mathcal{A}(\vec{r}, t)}{v} \frac{\partial \vec{J}(\vec{r}, t)}{\partial t} + \vec{\nabla} (\mu(\vec{r}, t) \phi(\vec{r}, t)) + \mu(\vec{r}, t) \mathcal{B}(\vec{r}, t) \Sigma_t(\vec{r}) \vec{J}(\vec{r}, t) = 0. \quad (\text{B4})$$

Appendix C: The Accuracy of $\alpha(\omega_{\text{eff}})$ and $\beta(\omega_{\text{eff}})$ Discontinuity Jump Conditions

In this appendix we introduce the accuracy of using the approximate variational analysis of the discontinuity jump condition that was introduced in [34, 44], comparing to the exact numerical two-region Milne problem solutions [33].

The exact energy density discontinuity $\rho_{2/1}$ is compared with the approximated β_1/β_2 (Fig. 12, along with Zimmerman's μ_1/μ_2) and the exact flux discontinuity $j_{2/1}$ is compared to α_1/α_2 (Fig. 13) as a function of ω_2 for two numerical values of ω_1 , 0.6 (a) and 0.95 (b).

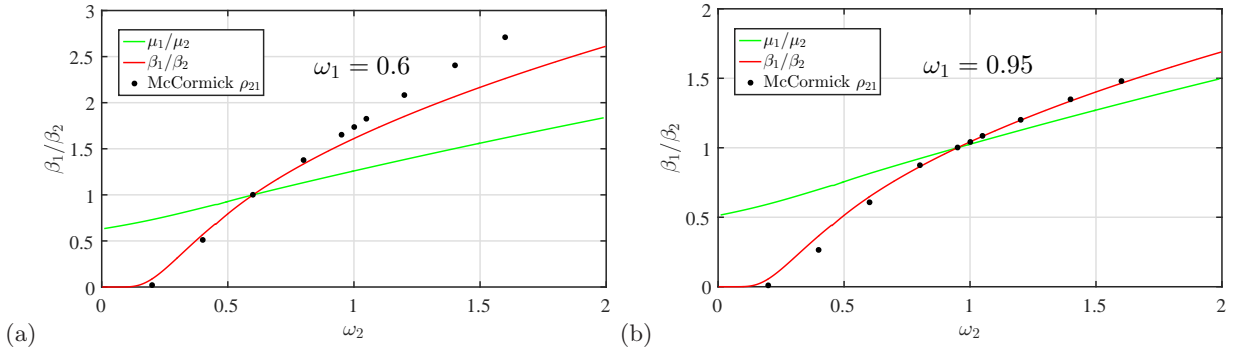


FIG. 12. The ratio β_1/β_2 , between two region, as a function of ω_2 using the exact McCormick solution [33] (black circles) and the approximate values of the variational analysis [34, 44] (red curves) for $\omega_1 = 0.6$ (a), and for $\omega_1 = 0.95$ (b).

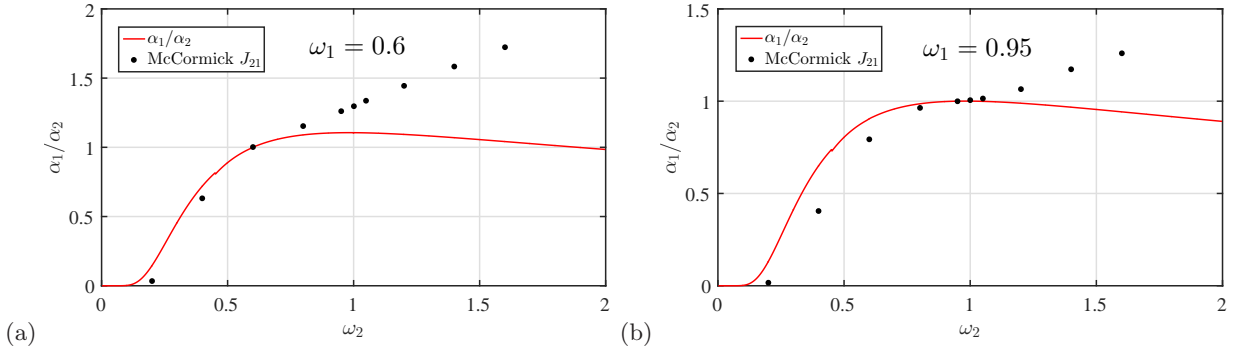


FIG. 13. The ratio α_1/α_2 , between two region, as a function of ω_2 using the exact McCormick solution [33] (black circles) and the approximate values of the variational analysis [34, 44] (red curves) for $\omega_1 = 0.6$ (a), and for $\omega_1 = 0.95$ (b).

We can see that the ratio between the zero moments ($E(\vec{r}, t)$) β_1/β_2 fits quite well along all the range to exact McCormick calculations. One should remember that μ_1/μ_2 (from Zimmerman's approximation) should not suppose to be similar to β_1/β_2 , since in the $\mu\mathcal{A}\mathcal{B}$ approximation we keep *only* the flux continuous (forcing $\alpha_1/\alpha_2 = 1$). The ratio between the first moments ($\vec{F}(\vec{r}, t)$) α_1/α_2 shows that when $\omega_2 < 1$, α_1/α_2 is also similar to the exact McCormick calculations, while for $\omega_2 > 1$, the accuracy decreases. However, the total accuracy of the approximate variational analysis to the exact solutions, is quite good.

In any case, the decrease of the McCormick exact $\rho_{2/1}$ and $j_{2/1}$, or the approximate variational analysis values, to zero when $\omega_2 \rightarrow 0$, makes it often numerically unstable, making the $\mu\mathcal{A}\mathcal{B}$ a preferable choice.

ACKNOWLEDGMENTS

We acknowledge the support of the PAZY Foundation under Grant No. 61139927. The authors thank Roe Kirschenzweig for using an IMC code for radiative problems, Stanislav Burov and the anonymous referees for their valuable comments.

-
- [1] B.Ya. Zel'dovich and P.Yu. Raizer, *Physics of shock waves and high temperature hydrodynamics phenomena*, (Dover Publications Inc. 2002).
- [2] J.D. Lindl, P. Amendt, R.L. Berger, S.G. Glendinning and S.H. Glenzer, *Phys. Plasmas* **11**, 339 (2004).
- [3] M.D. Rosen, *Phys. Plasmas*, **3**, 1803 (1996).
- [4] D. Mihalis and B.W. Mihalis, *Foundations of Radiation Hydrodynamics* (Oxford University Press, New York, 1984).
- [5] S. Chandrasekhar, *Monthly Notices of the Royal Astronomical Society*, **96**, 21 (1935).
- [6] E.A.Milne, *Monthly Notices of the Royal Astronomical Society*, **81**, 361 (1921).
- [7] C.A. Back, J.D. Bauer, J.H. Hammer, B.F. Lasinski, R.E. Turner, P.W. Rambo, O.L. Landen, L.J. Suter, M.D. Rosen, and W.W. Hsing *Phys. Plas.* **7**, 2126 (2000).
- [8] A.S. Moore, T.M. Guymer, J. Morton, B. Williams, J.L. Kline, N. Bazin, C. Bentley, S. Allan, K. Brent, A.J. Comley, K. Flippo, J. Cowan, J.M. Taccetti, K. Mussack-Tamashiro, D.W. Schmidt, C.E. Hamilton, K. Obrey, N.E. Lanier, J.B. Workman and R.M. Stevenson, *Journal of Quantitative Spectroscopy & Radiative Transfer*, **159**, 19 (2015).
- [9] R.E. Marshak, *Phys. Fluids* **1**, 24 (1958).
- [10] R. Pakula and R. Sigel, *Phys. Fluids* **28**, 232 (1985).
- [11] T. Shussman and S.I. Heizler *Phys. Plas.* **22**, 082109 (2015).
- [12] S.I. Heizler, T. Shussman and E. Malka *Journal of Computational and Theoretical Transport* **45**, 256 (2016).
- [13] G.C. Pomraning, *The Equations of radiation hydrodynamics*, (Pergamon Press 1973).
- [14] J. A. Fleck, and J.D. Cummings, *J. Comp. Phys.*, **8**, 313 (1971).
- [15] G.L. Olson, L.H. Auer, M. L. Hall, *J. Quant. Spectrosc. & Radiat. Transfer*, **64**, 619 (2000).
- [16] B. Su *Nuclear Science & Engineering* **137**, 281 (2001).
- [17] S.I. Heizler, *Nuclear Science & Engineering*, **166**, 17 (2010).
- [18] A.M. Winslow, *Nuclear Science & Engineering*, **32**, 101 (1968).
- [19] G.N. Minerbo, *Journal of Quantitative Spectroscopy & Radiative Transfer*, **20**, 541 (1978).
- [20] C.D. Levermore and G.C. Pomraning, *The Astrophysical Journal*, **248**, 321 (1981).
- [21] G.C. Pomraning, *A Comparison of Various Flux Limiters and Eddington Factors*, Lawrence Livermore Laboratory, University of California Livermore, UCID-19220 (1981).
- [22] G.C. Pomraning, *Journal of Quantitative Spectroscopy & Radiative Transfer*, **27**, 517 (1982).
- [23] C.D. Levermore, *Journal of Quantitative Spectroscopy & Radiative Transfer*, **31**, 149 (1983).
- [24] G.C. Pomraning, *Nuclear Science & Engineering*, **86**, 335 (1984).
- [25] K.M. Case, F. De Hoffmann G. Placzek, B. Carlson and M. Goldstein, *Introduction to The Theory of Neutron Diffusion - Volume I*, Los Alamos Scientific Laboratory (1953).
- [26] S.P. Frankel and E. Nelson, *Methods of Treatment of Displacement Integral Equations*, Los Alamos Scientific Laboratory, AEC-3497 (1953).
- [27] S.I. Heizler and P. Ravetto. *Transport Theory & Statistical Physics*, **41**, 304 (2012).
- [28] S.I. Heizler, *Transport Theory & Statistical Physics*, **41**, 175 (2012).
- [29] B.L. Koponen, R.J. Doyas, *Nuclear Science & Engineering*, **48**, 115 (1972).
- [30] A. Korn, *Nukleonik*, **9**, 237 (1967).
- [31] N.J. McCormick, *Nuclear Science & Engineering*, **37**, 243 (1969).
- [32] N.J. McCormick, R.J. Doyas, *Nuclear Science & Engineering*, **37**, 252 (1969).
- [33] R.J. Doyas, N.J. McCormick, *Transport-corrected boundary conditions for neutron diffusion calculations*, Lawrence Livermore Laboratory, University of California Livermore, UCRL-50443 (1968).
- [34] B.D. Ganapol, G.C. Pomraning, *Nuclear Science & Engineering*, **123**, 110 (1996).
- [35] G.B. Zimmerman, *Differencing asymptotic diffusion theory*, Lawrence Livermore Laboratory, University of California Livermore, UCRL-82792 (1979).
- [36] B. Su and G.L. Olson, *Ann. Nucl. Energy*, **24**, 1035 (1996).
- [37] B. Su and G.L. Olson, *Journal of Quantitative Spectroscopy & Radiative Transfer*, **62**, 279 (1999).
- [38] R.J. Doyas, B.L. Koponen, *Nuclear Science & Engineering*, **41**, 226 (1970).
- [39] G.C. Pomraning, *Nuclear Science & Engineering*, **21**, 62 (1965).
- [40] G.C. Pomraning, *Nukleonik*, **6**, 348 (1964).
- [41] R.P. Rulko, E.W. Larsen, *Nuclear Science & Engineering*, **114**, 271 (1993).
- [42] R.G. McClarren, J.P. Holloway, T.A. Brunner, *Journal of Quantitative Spectroscopy & Radiative Transfer*, **109**, 389 (2008).
- [43] M. Murakami, J. Meyer-Ter-Vehn and R. Ramis, *Journal of X-ray Science & Technology* **2**, 127 (1990).
- [44] G.C. Pomraning, R.P. Rulko, B. Su, *Nuclear Science & Engineering*, **118**, 1 (1994).